Multi-objective sensitivity analysis of shell-and-tube LHTES performance

Francesco Fornarelli[1,*] and *Lorenzo* Dambrosio[2,†].

[1]University of Foggia, Department of Sciences of Agriculture, Food, Natural Resources and Engineering, 71121, via Napoli 25, Foggia, Italy
[2]Polytechnic University of Bari, Department of Mechanics, Mathematics and Management, 70125 via Orabona 4, Bari, Italy

Abstract. In the present paper a sensitivity analysis has been carried out concerning the charging/discharging time and the stored energy performances of a shell-and-tube LHTES with respect to the number of tubes and the tube internal radius. The aim of this analysis is to investigate how the design variables affect the LHTES performance. this could lead to determine the thermal storage optimal design. Thus, the sensitivity analysis has a key role in the selection of several acceptable solutions. The considered *LHTES* exhibits a cylindrical shell geometry characterized by constant height and diameter. This aspect has allowed to employ simplified theoretical models able to predict the charging/discharging time and the stored energy performance. These models consider a constant heat exchange wall temperature whereas the heat exchange area and the whole *PCM* volume vary according to the design variables. This analysis represents the first step to solve the multi-objective optimization of the thermal storage design problem and then to determine the best solutions in both design variables and thermal storage performance domains.

1 Introduction

The continuous growth of energy demand on planetary scale leads to a complete rethinking of the energy production, transport, and final exploitation. Although the efficiency improvement mitigated the primary energy source requirement, the ecological footprint of the energy sector needs to be reduced. The key to get this point passes through the increasing of the renewable energy share and the reduction of exergy waste. Thus, even if the technologies to convert the renewable energy sources can compete with fossil fuel power plant, the uncertainty of their availability represents the main issue to manage. Specifically, solar energy is mostly influenced by the circadian cycle as well as seasonal and weather conditions. Hence, the operational flexibility of a solar power plant needs to be improved with respect to primary source availability. Both, photovoltaic and Concentrated Solar Power (CSP) intermittency can be dumped by means of energy storage (e.g., batteries and thermal storage) [1, 2]. Indeed, in CSP applications, where a thermal power block is usually coupled with, the thermal storage is the implemented technology. The power block influences the temperature ranges such as classical steam Rankine cycle or Organic Rankine Cycle (ORC) that require different operating temperatures [2, 3]. Therefore, the temperature range of the stored heat in the thermal storage device represents a first main classification of such devices. The amount of heat strictly depends on the application, however, in usual power plant applications its size is huge and deserve being minimized. Thus, phase change materials (PCMs) have been considered, where the latent heat of the phase change can be used increasing its specific heat content. These devices are called Latent Heat Thermal Energy

* Corresponding author: francesco.fornarelli@unifg.it
† Corresponding author: lorenzo.dambrosio@poliba.it

Storage (LHTES). The PCM is chosen according to its melting temperature that has to match the operating temperature of the application, i.e. the power block. Moreover, the solid-liquid phase change promotes the triggering of convective heat transfer improving the performance of the storage [5]. The convective motion is then influenced not only by the physical characteristics of the PCM but also by the geometrical and operating parameters [6, 7]. Hence, the characteristic times of charging and discharging are sensibly different and can change according to the geometrical configuration of the device [8]. The parameters influencing the device performance are often competing with respect to the objectives. For this purpose, several approaches can be implemented [9-12]. Thus, a sensitivity analysis represents a first step to set an optimization procedure to support the LHTES design. Here, a sensitivity analysis on the main characteristic parameters of the shell-and-tube LHTES is performed considering the capacity and characteristic times as storage performance.

2 Numerical model

The device performance is predicted by means of an integral form of the energy conservation equation. The Heat Transfer Fluid (HTF) exchange heat to the storage material (PCM) with three main mechanisms: forced convection, conduction, and natural convection. The forced convection concerns the HTF imposed flow rate through the inner tube. According to the experiments, usually, the flow rate is high enough to limit the temperature difference between the inlet and the outlet. Moreover, the HTF inner tube has a low thermal resistance with respect to the PCM. Thus, in a first approximation, the temperature of the inner tube has been considered constant along the height of the LHTES. Moreover, the model must consider different thermal behaviour of the solid and the liquid fraction of the PCM together with the phase change. Then, the PCM stores heat according to the temperature change of the solid and the liquid fraction, the sensible share, and thanks to the phase change rate, the latent share. Due to the different behaviour of the LHTES shell-and-tube device oriented in vertical position two different models has been implemented to predict the overall charging and discharging time of the thermal storage device. The charging and discharging models here implemented are those proposed by Fornarelli et al. [13] and Fornarelli & Camporeale [14], respectively. Here, the PCM consists of a binary mixture of 60% of $NaNO_3$ and 40% of KNO_3 where the latent heat is $\Lambda = 110000\, J/kg$, the conductivity is $k = 0.4886\, W/(mK)$ the dynamic viscosity in the operative range is $\mu = 7.008\ 10^{-3} kg/(ms)$, the specific heat is $c_p = 1626\, J/(kgK)$ and the density is $\rho = 1994\, kg/m^3$. The charging phase assumes that the HTF temperature is always above the melting temperature of the PCM, therefore the heat transfer at the wall on the PCM side is strictly convective. The overall charging time, t_{charge}, can be calculated considering the balance between the heat transfer at the wall and the sensible and latent heat stored in the PCM:

$$t_{charge} = \frac{VH}{A\alpha}\frac{1}{Nu}\left(ln\frac{T_{in}-T_w}{T_{sol}-T_w} + \frac{1}{Ste} + ln\frac{T_{liq}-T_w}{T_{fin}-T_w}\right) \quad (1)$$

The model includes the geometrical parameter of the device, where V, A and H represent the PCM volume, the heat exchange area between the heated wall and the PCM and the height of the heat exchange wall, respectively. α is the thermal diffusivity, Nu is the Nusselt number, $Ste = c_p(T_w - T_{liq})/\Lambda$, the Stefan number, is defined as the ratio between the sensible and the latent heat of solidification/melting of the PCM. T_{in}, T_{fin} are the initial and the final average temperature of the PCM, whereas T_{liq} and T_{sol} are the liquidus and solidus

temperature when the phase change occurs. In the cases here discussed the $T_{liq} = 517.3\ K$ and $T_{sol} = 493.0\ K$. For the charging phase here $T_{in} = 423.15\ K$, and $T_{fin} = 0.994T_w$, with $T_w = 523.15K$. Hence, the convective heat transfer coefficient can be estimated according to well-known Nusselt Rayleigh correlations. The overall discharging time, t_{dis}, is likewise predicted considering the heat transfer from the PCM to the wall, where the temperature is maintained below the solidus temperature. In this case the convective heat transfer is in the external zone of the PCM, since the one closest to the heat exchange wall is solid. From the different contributions of the discharging process the overall discharging time reads:

$$t_{dis} = \frac{r_i V H}{r_m A \alpha} \frac{1}{Nu} \left(ln \frac{T_{in} - T_w}{T_{liq} - T_w} \right) + \frac{\Lambda}{c_p (T_w - T_{liq})} \frac{1}{\alpha} \left[\frac{(r_e^3 - r_i^3)}{3 r_i} - \frac{(r_e^2 - r_i^2)}{2} \right] + \frac{V}{A} \frac{1}{\alpha} \frac{r_e - r_i}{2} ln \frac{T_w - T_{sol}}{T_w - T_{fin}} \quad (2)$$

Other geometrical parameters used in the model are: r_i, r_e and $r_m = \frac{r_i + r_e}{2}$ are the internal wall radius, the radius of the external shell where the PCM is enclosed and the mean radius, respectively. For the discharging process $T_{in} = 523.15\ K$ and $T_{fin}$is the temperature of the PCM at r_m considering the temperature distribution across the solid PCM with $T(r_i) = T_w = 473.15K$ and $T(r_e) = T_{sol}$ [14].

3 Latent Heat Thermal Energy Storage geometries

The described models consider a constant heat exchange wall temperature whereas the heat exchange area, *A*, the whole Phase Change Material (*PCM*) volume, *V* vary according to the design variables (the number of tubes and the tube internal radius). Moreover, similarly to case of the simplified model of the single module of the *LHTES*, the model of multi tubes case treats the external shell adiabatic and the wall temperature constant. The following geometric constraints have been adopted in both charging and discharging models:

- cylindrical geometry with height equal to diameter (H=D=840.146 *mm*);
- the tubes radius varies from a minimum value (flat plate condition), r_{min}, to a maximum value (tubes tangential condition), r_{max}, which depends on the selected configuration.

As stated, the minimum radius value derives from the flat plate condition, which, in turns, is just a function of cylindric shell height. Therefore, the r_{min} values is given by [15]:

$$r_{min} = \frac{1}{2} \frac{f(Pr)}{Gr^{1/4}} \quad (3)$$

where

$$f(Pr) = 11.474 + 48.92/Pr^{0.5} - 0.006085/Pr^2 \quad (4)$$

In the present case, r_{min}*=45.476 mm* for the charging time model, whereas it assumes the value of *67.6 mm* for the discharging time. Such a discrepancy is due to the dependence of the Grashof number from Rayleigh number which, in turn, is a function of the initial temperature of thermal fluid which is different for the charging and discharging phases.

For a 4-modules configuration (Fig. 1a), the relation between the shell diameter and maximum tube radius is given by the

$$D = 2\, r_{max} \left(1 + \sqrt{2}\right) \quad (5)$$

from which emerges that r_{max}*=174 mm*. It is noticeable that a few *LHTES* parameters are function of the number of tubes and their internal radius such as the heat exchange area and the *PCM* volume that can be expressed as:

$$A = m\ 2\ \pi\ r_i H$$
$$V_{PCM} = \frac{\pi}{4}\ H^3 - m\ \pi\ r_i^2 H \tag{6}$$

where *m* represents the tubes number.

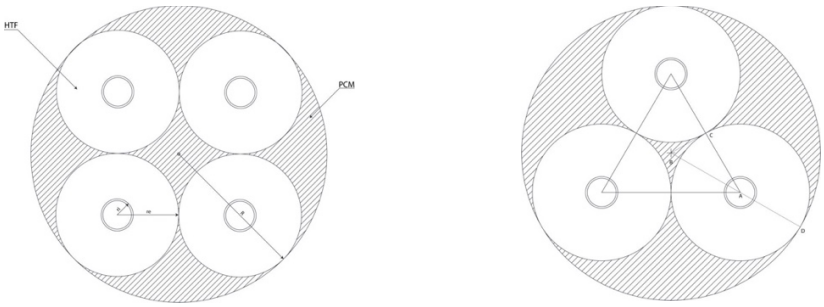

a ***b***

Fig. 1. 4-modules configuration (*a*), 3-modules configuration (*b*). Maximum and minimum tubes radius.

$$D = 2\ r_{max}\left(1 + \sqrt{2}\right)$$

$$A = m\ 2\ \pi\ r_i H$$
$$V_{PCM} = \frac{\pi}{4}\ H^3 - m\ \pi\ r_i^2 H$$

Figure 1b shows the 3-modules configuration; in this case, it is quite straightforward to determine the relation between the maximum tube radius and that of the 4-modules configuration (Eq. 2) as:

$$r_{max} = (r_{max})_4 \frac{(1+\sqrt{2})\sqrt{3}}{\sqrt{3}+2} \tag{7}$$

Eq. 4 allows to determine the maximum tube radius is equal to r_{max}*=195 mm*.

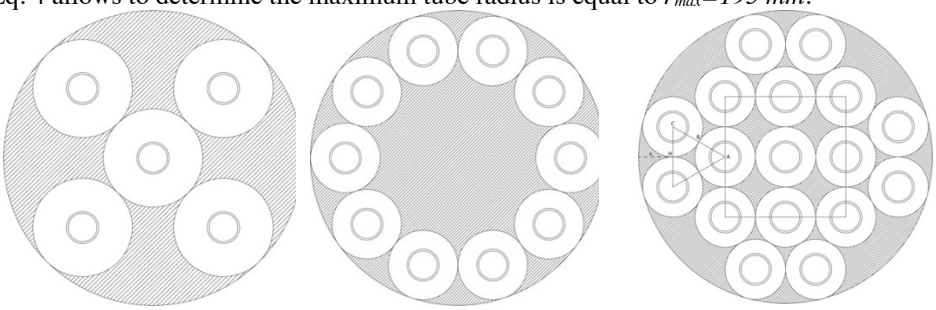

a ***b*** ***c***

Fig. 2. 5-modules configuration (*a*), 10-modules configuration (*b*) and 17-modules configuration (*c*). Maximum and minimum tubes radius.

Figures 2a and 2b report the 5-modules and 10-modules configuration, respectively. From some geometrical relations, the maximum tube internal radii for the two configurations are, respectively, given by

$$r_{max} = (r_{max})_4 \frac{1 + \sqrt{2}}{3} \tag{8}$$

$$r_{max} = \frac{R'}{2}\left(\sqrt{\frac{5}{4}} - \frac{1}{2}\right) \tag{9}$$

where

$$R' = (r_{max})_4 \frac{4\left(1+\sqrt{2}\right)}{\sqrt{5}+3} \tag{10}$$

being $(r_{max})_4$ the 4-modules maximum tube radius (Eq. 2).

Figure 2c depicts the tubes distribution for a 17-modules *LHTES*, where the following approximate formula for the maximum tube radius can be adopted:

$$r_{max} = (r_{max})_4 \frac{1+\sqrt{2}}{3+2\,cos(30)} \tag{11}$$

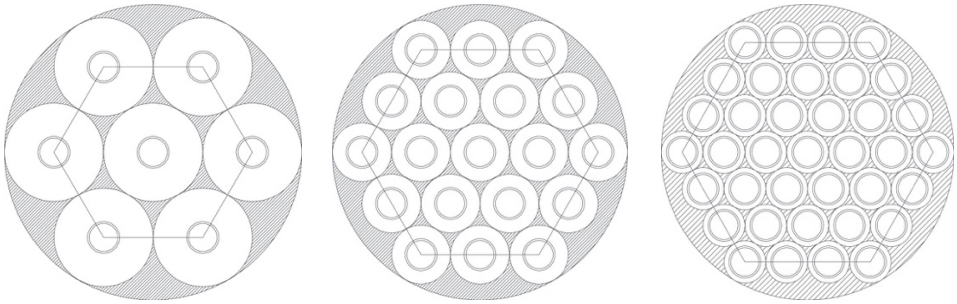

a ***b*** ***c***

Fig. 3. 7-modules configuration (*a*), 19-modules configuration (*b*) and 37-modules configuration (*c*). Maximum and minimum tubes radius.

Finally, figures 3a, 3b and 3c illustrate the solutions with 7-modules, 19-modules and 37-modules, respectively, following a honeycomb tubes distribution. In this case, the relation between the shell radius and maximum tube radius is given by the generic formula:

$$r_{max} = \frac{R}{1+2\,a} \tag{12}$$

where *a* represents a selective factor that indicates the number of circumscribed hexagons. Tab. 1 summarize the maximum tube internal radius for 7, 19 and 37 modules.

Table 1. Maximum tube internal radius for a honeycomb tubes distribution.

Number of modules	*a*	r_{max}
7	1	$R/3$
19	2	$R/5$
37	3	$R/7$

4 Sensitivity Analysis Results

The aim of this work is to investigate the design performance of a Latent Heat Thermal Energy Storage when the design variables are varied. Considering the thermal storage configurations in the previous paragraph, it is straightforward to choose as design variables the internal tubes radius, r_i and the number of modules *N*, while keeping the shell geometry constant. As far *LHTES* performance is concerned, it is important to note that such devices should permit not only an easy heat transfer from the Heat Transfer Fluid (HTF) and but also a large energy storage. For these reasons, the selected performance variables are represented by the total energy stored into the device, the charging and discharging time. In the present work, only the *LHTES* configuration described in the previous paragraph will be taken into

account. Of course, this analysis represents a first step towards the multi-objective optimization *LHTES* design; therefore, different geometry, different modules arrangements and even a not constant modules' internal radius distribution are possible, but they are beyond the scope of this work. From the simplified model described in section 2, applied to a multi-tube configuration, it has been possible to determine how the *LHTES* performance variables change when the design variables (internal tubes radius, r_i and the number of modules N) vary in their respective intervals. Figure 9 reports the results of such analysis in *LHTES* performance Energy Stored, Charging Time plane:

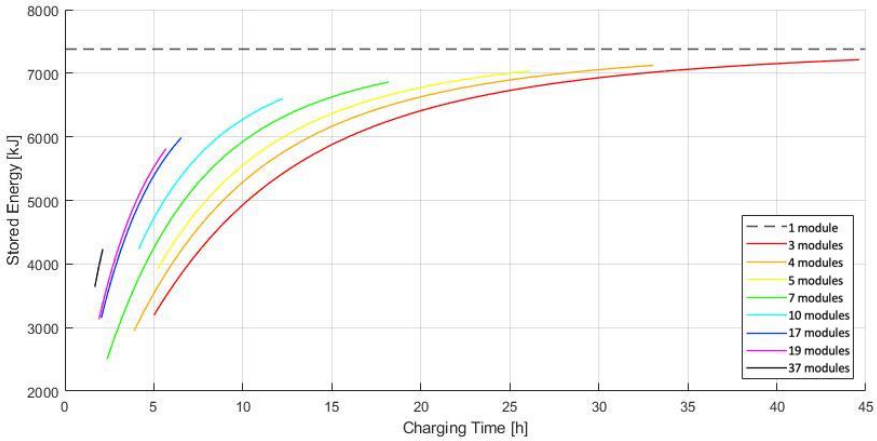

Fig. 4. *LHTES* performance in Energy Stored, Charging Time plane according to the HTF radius changing.

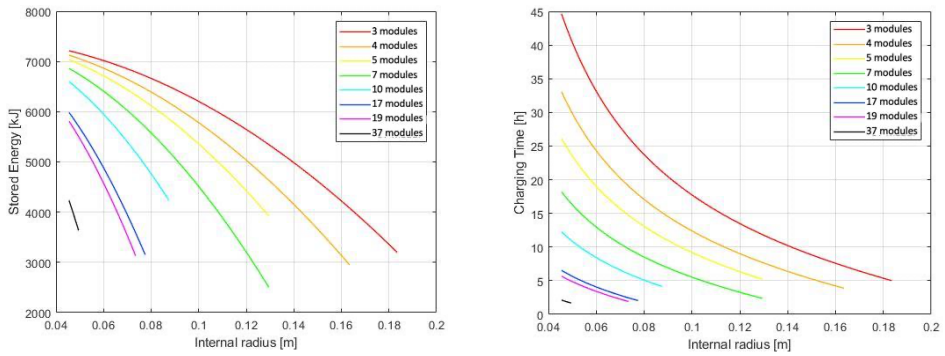

a ***b***

Fig. 5. *LHTES* Energy Stored (*a*) and *LHTES* Charging (b) vs. module internal radius

Observing Fig. 4, it is possible to note that the greater is number of modules the smaller is the *LHTES* stored energy and the shorter is the Charging Time. This is because, when the number of modules is increased, for a fixed shell geometry, the volume available for *PCM* is reduced. Another consequence is that the heat exchange area is also increased and therefore the ratio *PCM* volume to heat exchange area is further reduced: this leads to a shorten of the Charging Time. Moreover, the dashed line in Fig. 4 indicates the *LHTES* stored energy for single minimum radius module; this energy level represents the maximum storable energy limit. For completeness, figures 5a and 5b illustrate the dependency of both *LHTES* performance variables with respect the tubes internal radius and the number of modules.

Moreover, a second results' analysis, regarding the Discharging Time has been also carried out. This is because the thermal storage devices are often employed in the

Concentrated Solar Power (*CSP*) plants during night and to avoid lacks in power supply the Discharging Time plays a crucial role in the design of thermal storage devices used in *CSP* plants. Figure 6 illustrates the analysis of *LHTES* performance in terms of Energy Stored, Discharging Time for the configurations examined in section 3:

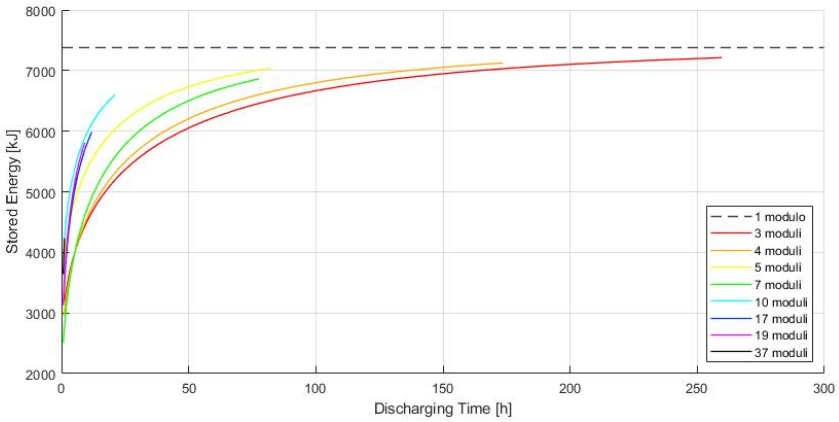

Fig. 6. *LHTES* performance in Energy Stored, Discharging Time plane

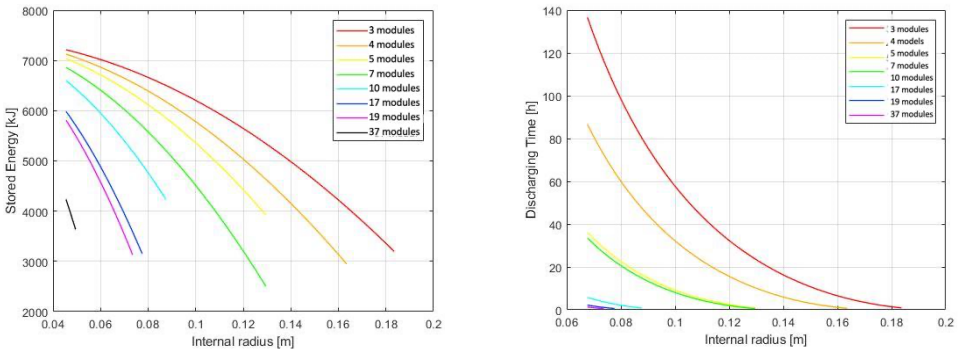

a ***b***

Fig. 7. *LHTES* Energy Stored (*a*) and *LHTES* Discharging Time (*b*) vs. module internal radius

Also in this case, the increase in the number of modules results in a lower *PCM* volume. Likewise, the previous analysis, this affects both the Stored Energy and the Discharging Time, as shown in Fig. 6. Figures 7a and 7b report the influence of the single *LHTES* performance variables with respect the tubes internal radius and the number of modules. As final consideration, such analyses will be very useful to carry out a multi-objective optimization design. In fact, each point in fig. 4 and 6 represent a candidate design solution, and therefore, for given requirements in terms of Stored Energy, Charging and Discharging Time, the design solution is not unique. To evaluate the best candidate design solution, all the not-dominated solutions have to be detected or, in other words, among all the candidate design solutions, the best solution are those whose single performance can't be improved without degrading some others.

Conclusions

In the present paper a sensitivity analysis has carried out considering the stored energy and the charging/discharging time performance of a shell-and-tube latent heat thermal energy storage with respect to the number of modules and the tube internal radius. Due to the features

of the considered thermal storage devices, a simplified model of a Latent Heat Thermal Energy Storage with a cylindrical shell geometry has been considered. The purpose of this study was to explore the design variable field which in turn impacts significantly on the multi-objective thermal storage optimal design. In fact, the geometry of the PCM shell and the heat exchange area affect the design performance of such devices, and for this reason the candidate design solution is not unique. Thus, the proposed sensitivity analysis plays an essential role since for the specific application the design of such devices could lead to several acceptable solutions. In future works, to evaluate the best candidate design solution, all the not-dominated solutions have to be detected

References

1. D. Feldman, R. Margolis, Q1/Q2 Solar Industry Update, Tech. rep., National Renewable Energy Laboratory, NREL/PR-6A20-74585 (2019).
2. S.M. Hasnain, Energ Convers. Manage. **39**, 11:1127–38 (1998).
3. D. Thanganadar, F. Fornarelli, S. Camporeale, F. Asfand, K. Patchigolla, Appl. En., **282**, art. no. 116200 (2021).
4. E. A. Bufi, S. Camporeale, F. Fornarelli, B. Fortunato, A.M. Pantaleo, A. Sorrentino, M. Torresi, En. Proc., 126, pp. 429-436 (2017).
5. F. Fornarelli, S. Camporeale, B. Fortunato, M. Torresi, P. Oresta, L. Magliocchetti, A. Miliozzi, G. Santo, Appl. Energy 164 711–722 (2016).
6. F. Fornarelli, M. Valenzano, B. Fortunato, S. Camporeale, M. Torresi, P. Oresta, En. Proc. **148,** 471–478 (2018)
7. F. Fornarelli, V. Ceglie, B. Fortunato, S. Camporeale, M. Torresi, P. Oresta, A. Miliozzi, En. Proc. **126**, 501–508 (2017).
8. F. Fornarelli, M. Torresi, P. Oresta, L. Dambrosio, A. Miliozzi, S.M. Camporeale AIP Conf. Proc., 2191, art. no. 020079 (2019).
9. L. Dambrosio, R. Micera, B. Fortunato, M. Torresi, En. Proc., **148**, 1050-1057, (2018)
10. L. Dambrosio, B. Fortunato, M. Torresi, S.M. Camporeale, F. Fornarelli, En. Proc., **126**, 533-540, (2017)
11. L. Eriksson, E. Johansson, N. Kettaneh-Wold, C. Wikstrm, S. Wold *Design of Experiments: Principles and Applications* (Umetrics Accademy 2000).
12. M. Caramia, P. Dell'Olmo, *Multi-objective Management in Freight Logistics* Springer (Science & Business Media 2008).
13. F. Fornarelli, S. Camporeale, B. Fortunato, Appl. Therm. Eng. 153, 51–57 (2019).
14. F. Fornarelli, S. Camporeale, Appl. Therm. Eng. 179, 115709 (2020).
15. C. Popiel, J. Wojtkowiak, K. Bober, Exp. Therm. Fluid Sci. 32 (2) 607–613 (2007)